Isotope effect for the mutual neutralization reaction at low collision energies: $He^+ + H^-$

A. Dochain,[1,2,*] V. M. Andrianarijaona,[3] and X. Urbain[1,†]

[1]*Institute of Condensed Matter and Nanosciences, Université Catholique de Louvain, B-1348 Louvain-la-Neuve, Belgium*

[2]*Department of Physics, Stockholm University, Stockholm 10691, Sweden*

[3]*School of Engineering and Physics, Southern Adventist University, Collegedale, Tennessee 37315, USA*

(Received 2 June 2023; accepted 18 September 2023; published 16 October 2023)

We measured the branching ratios of the $He^+ + H^-$ and $He^+ + D^-$ mutual neutralization at a collision energy below 25 meV. Those are correctly reproduced using the Landau-Zener model applied to potential energy curves computed by an anion-centered asymptotic model. The analyticity of both models allows getting a deeper insight into the reaction. It allows defining a low collision energy regime for the mutual neutralization at which the collision energy no longer affects the branching ratios. Using those models, we explain how heavier isotopes favor the production of higher excited states.

DOI: 10.1103/PhysRevA.108.042809

I. INTRODUCTION

Mutual neutralization (MN) recently gained an increased focus, following the discovery of its effect on the late-type stars' apparent metallicity (see [1,2] and references therein). This led to a large number of theoretical studies dealing with $X^+ + H^-$ mutual neutralization [1,3–33], focusing on collision energies below 10 000 K, i.e., 1 eV.

In order to confirm those calculations, recent measurements were also performed [6,34–38], but due to technical limitations of the merged beam setups both at UCLouvain [39] and at DESIREE [40], the mass ratio between the anion and the cation was limited. Therefore $X^+ + D^-$ MN reactions were used as a proxy for $X^+ + H^-$, leading to difficulties in the comparison between theoretical and experimental results, as the isotope effect might have to be taken into account [41].

This paper describes this isotope effect on MN at low collision energies using the analytical two-channel Landau-Zener (SLZ) model with the $He^+ + H^-/D^-$ MN reaction taken as an example. Merged beam experiments are reported that validate this approach.

II. EXPERIMENTAL SETUP

In order to measure the isotope-dependent branching fractions, we used our single-pass merged beam setup as described by Launoy *et al.* [6] and shown in Fig. 1. The He^+ beam is generated by an electron cyclotron resonance ion source and the $H^-(D^-)$ beam is generated by a duoplasmatron source fed with $H_2(D_2)$ gas. The anion and cation beams are merged in an observation cell. A biasing voltage applied to the cell defines the collision energy $E_{r,i}$. The neutralized ions are collected by a pair of time and position sensitive detectors (microchannel plates in a Z-stack configuration, and equipped with a resistive anode). The simultaneous measurement of the positions and times of arrival of the He and H(D) products allows us to reconstruct the momentum vector of the He-H pseudoparticle, leading to the determination of the center-of-mass frame kinetic energy $E_{r,f}$. The kinetic-energy release (KER) $E_{\mathrm{KER}} = E_{r,f} - E_{r,i}$ allows us to identify the products of the reaction using

$$E_{\mathrm{KER}} = [I(\mathrm{He}) - {}^eA(\mathrm{H})] - [E_{\mathrm{lev}}(\mathrm{He}) + E_{\mathrm{lev}}(\mathrm{H})]$$

where $I(\mathrm{He}) = 24.5874$ eV is the helium ionization potential, ${}^eA(H) = 0.754$ eV is the hydrogen electron affinity, and E_{lev} is the energy level of the produced atomic state. Those energy levels are retrieved from the NIST-ASD database [42] and the associated E_{KER} is displayed in Table I. The experimental spectra are displayed in Fig. 2 and the fitted branching ratios are listed in Table I.

III. THEORY

In order to describe the results, we computed the interaction terms between the diabatic potential energy curves using an anion-centered asymptotic model (ACAM) similar to the one described by Janev [44] but with an accurate description of the asymptotic form of the H^- wave function [45] and a slightly different description of angular momentum (see Appendix A).

The dynamics of the collision was computed using the two-channel [46] and multichannel [47] Landau-Zener (MLZ) models ($\mathrm{ACAM_{SLZ}}$ and $\mathrm{ACAM_{MLZ}}$). While the latter gives a better quantitative description of the reaction (details are given in Appendix B) and gives results similar to the one obtained by Larson *et al.* [4], the two-channel version $\mathrm{ACAM_{SLZ}}$ remains purely analytical, which allows for a qualitative description of the isotope effect.

*arnaud.dochain@fysik.su.se

†xavier.urbain@uclouvain.be

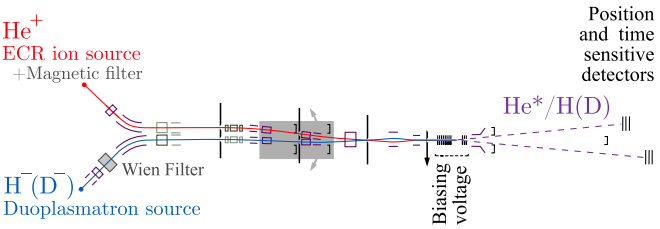

FIG. 1. Schematics of the single-pass merged beam setup.

Using this model, and averaging over the Stueckelberg oscillations, the partial cross section is given by [46,48,49]:

$$\sigma_{\mathrm{SLZ}} = 4\pi R_x^2 \left(1 - \frac{V(R_x)}{E_{r,i}}\right) G(\zeta) \tag{1}$$

where

$$G(\zeta) = \int_1^\infty e^{-\zeta x}(1 - e^{-\zeta x})\frac{dx}{x^3} \tag{2}$$

TABLE I. Branching ratios for $He^+ + H^-$ (top) and $He^+ + D^-$ (bottom) reactions and associated E_{KER}. Only the neutralized cation state is given as no excited hydrogen states were observed. The 1-σ error is indicated in parentheses. The theories are given at a collision energy of 10 meV; the experimental average collision energy for the $He^+ + H^-$ (D^-) is 13 meV (23 meV). Comparison between $\mathrm{ACAM_{SLZ}}$ and $\mathrm{ACAM_{MLZ}}$ is given in Table II of Appendix A. The partial cross sections and the reaction rates of $\mathrm{ACAM_{MLZ}}$ are given in the Supplemental Material [43].

He state	E_{KER} (eV)	Experiment (H^-)	$\mathrm{ACAM_{MLZ}}$	Larson *et al.* [4]
$2s\ ^3S$	4.0138		0.00	0.00
$2s\ ^1S$	3.2175		0.00	0.03
$2p\ ^3P^o$	2.8693	0.01(0.01)	0.00	0.05
$2p\ ^1P^o$	2.6154	0.00(0.01)	3.54	0.58
$3s\ ^3S$	1.1149	49.93(2.54)	48.55	48.58
$3s\ ^1S$	0.9131	10.08(1.96)	12.17	10.37
$3p\ ^3P^o$	0.8263	21.89(1.25)	24.66	28.84
$3d\ ^3D$	0.7597	14.48(1.00)	5.01	3.65
$3d\ ^1D$	0.7593		1.70	2.88
$3p\ ^1P^o$	0.7464		4.37	4.93
$4s\ ^3S$	0.2394	0.00(0.00)	0.00	

He state	E_{KER} (eV)	Experiment (D^-)	$\mathrm{ACAM_{MLZ}}$	Larson *et al.* [4]
$2s\ ^3S$	4.0138		0.00	0.00
$2s\ ^1S$	3.2175		0.00	0.01
$2p\ ^3P^o$	2.8693	0.85(0.29)	0.00	0.05
$2p\ ^1P^o$	2.6154	1.58(0.29)	1.08	0.34
$3s\ ^3S$	1.1149	42.80(0.76)	43.00	43.88
$3s\ ^1S$	0.9131	11.35(0.35)	14.11	10.89
$3p\ ^3P^o$	0.8263	27.05(0.53)	28.27	31.31
$3d\ ^3D$	0.7597	13.28(3.66)	6.09	4.13
$3d\ ^1D$	0.7593		2.09	3.68
$3p\ ^1P^o$	0.7464		5.35	5.86
$4s\ ^3S$	0.2394	0.43(0.40)	0.00	0.00

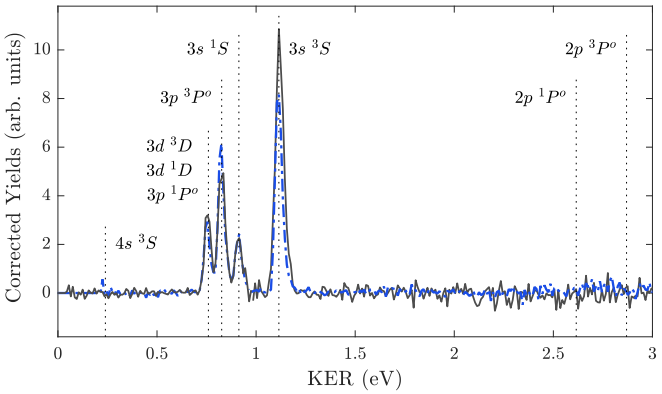

FIG. 2. Experimental kinetic-energy release spectra: He^+(12.5 keV)+H^-(2.5 keV) in black and He^+(11.5 keV)+D^-(6.5 keV) in blue. The collision energies are 13 and 23 meV respectively.

is a highly nonlinear function of the collision energy (see Fig. 4);

$$\zeta = \frac{2\pi E_{ic}^2}{\hbar \Delta F v_{r,i}\sqrt{1 - V(R_x)/E_{r,i}}} \tag{3}$$

where E_{ic} is the interaction potential between the ionic (i) and covalent state (c) whose diabatic potential energy curves are V_i and V_c, respectively; R is the internuclear distance; R_x is the internuclear distance at which $V_c(R_x) = V_i(R_x) = V(R_x)$; $\Delta F = |d/dR(V_c - V_i)|$; and $v_{r,i}$ is the initial collision velocity.

IV. LOW COLLISION ENERGY REGIME

As theory and experiment are in a satisfactory agreement, it is possible to explain the difference between $He^+ + H^-$ and $He^+ + D^-$ MN branching fractions. This would require us to define the low collision energy regime and its approximation, then deriving Eqs. (1) and (3) at low collision energy. It allows explaining why the difference in the collision energy (experimental) does not really matter for the branching fraction measurement. And finally, as all those aspects of the experiment can be put aside, it is possible to isolate this isotope effect on the atom-atom mutual neutralization at low collision energies.

But, before discussing the low collision energy approximation for the MN, it is useful to deduce the MN partial cross section in the high collision energy regime, defined as

$$E_{r,i} \gg E_{\mathrm{KER}} = -V(R_x). \tag{4}$$

In this case, the cross section is approximately

$$\sigma_{\mathrm{SLZ}} \simeq 4\pi R_x^2 G\left(\frac{2\pi E_{ic}^2}{\hbar \Delta F v_{r,i}}\right), \tag{5}$$

which means that the collision is described by the collision velocity instead of the collision energy.

Let us now define what the "low collision energy" regime is for the MN; in this paper we define it as

$$E_{r,i} \ll E_{\mathrm{KER}} = -V(R_x). \tag{6}$$

In the $He^+ + H^-/D^-$ MN case, this corresponds to collision energies below 50 meV.

In such case, Eqs. (1) and (3) become

$$\sigma_{\mathrm{SLZ}} \simeq 4\pi R_x^2 \frac{E_{\mathrm{KER}}}{E_{r,i}} G(\zeta) \tag{7}$$

and

$$\zeta \simeq \frac{2\pi E_{ic}^2}{\hbar \Delta F v_{r,i} \sqrt{2E_{\mathrm{KER}}/\mu v_{r,i}^2}} = \frac{2\pi E_{ic}^2}{\hbar \Delta F} \sqrt{\frac{\mu}{2E_{\mathrm{KER}}}} \tag{8}$$

where μ is the reduced mass of the atoms.

As shown in Eq. (8), there is no collision energy dependence of ζ, which means—as stated in Eq. (7)—that the partial cross section is inversely proportional to the collision energy, i.e., the predicted cross section follows the well-known $1/E_{r,i}$ dependence—instead of the velocity dependence mentioned above.

These equations also show that the branching ratio remains constant at low collision energies. In order to show that, let us estimate the branching ratio for a system—where two output channels 1 and 2 are accessible—at two collision energies $E'_{r,i}$ and $E''_{r,i}$. Using the fact that $\zeta_1(E'_{r,i}) = \zeta_1(E''_{r,i}) = \zeta_1$ and $\zeta_2(E'_{r,i}) = \zeta_2(E''_{r,i}) = \zeta_2$, the branching ratio for the state $k = 1, 2$ is

$$\frac{\sigma_k}{\sigma_1 + \sigma_2} = \frac{R_{x,k}^2 E_{\mathrm{KER},k} G(\zeta_k)}{R_{x,1}^2 E_{\mathrm{KER},1} G(\zeta_1) + R_{x,2}^2 E_{\mathrm{KER},2} G(\zeta_2)} \tag{9}$$

where all the collision energy factors simplify. This also means that the actual collision energy at which the branching ratios are measured does not matter, as long as this collision energy satisfies Eq. (6). This also validates the experiment, as the merged beam experiments performed at low collision energies always have some collision energy spread. This spread is often non-negligible, but as the branching ratios are not sensitive to the collision energy in this collision energy regime, the spread does not affect the branching ratios measured experimentally.

Another equivalent description is that the MN reaction is mainly driven by the Coulomb potential, meaning that the "trajectories" (or wave propagation) follow the electrostatic approximation. It means that for a given collision energy, the trajectories do not depend on the mass of the ions. Furthermore, the Landau-Zener model states that the transition probability at the crossing depends on the velocity at the crossing but, as the collision energy is much smaller than the kinetic energy gained at the crossing, the velocity at the crossing does not depend on the collision energy, meaning that this component of the cross section remains constant.

V. ISOTOPE EFFECT

It remains to describe the isotope effect on the reaction, which is given by a $\sqrt{\mu}$ factor in Eq. (8). The identification of the reduced mass as a driving parameter of the isotope effect has already been highlighted by Belyaev and Voronov [50]. They identified two concurring isotope effects, one of them being the increase of the maximum angular momentum for heavier systems, and the other a reduction of the Landau-Zener transition probability $e^{-\zeta}$ for the same systems due to reduced radial velocities at the crossing point.

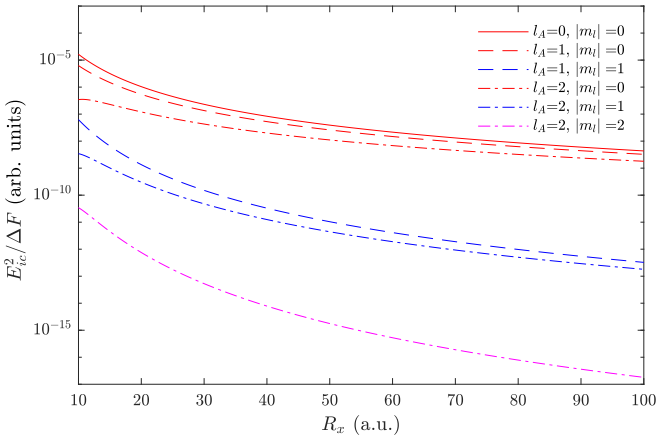

FIG. 3. The internuclear crossing distance dependence of the interaction term.

In this section, we describe the isotope effect as a single nonlinear dependence on ζ instead of two opposing effects which should be balanced to maximize the (total or partial) cross section. But before discussing the effects of the reduced mass on the total cross section, one should remember that this discussion is about all possible output channels of any low collision energy MN reaction. One cannot make the analysis for a given value of $\{E_{ic}, \Delta F\}$ but must take into account all the possible values of $\{E_{ic}, \Delta F\}$. Therefore, it is useful to use the ACAM model to estimate the interaction term whose tendency is shown in Fig. 3.

In that figure, one can see that, for the crossing radius range where the ACAM is valid ($R_x > 10$ a.u.), $E_{ic}^2/\Delta F$ decreases monotonically. It also shows that there is a strong dependence of this term on the value of m_l which suggests that it might not be possible, *a priori*, to determine the isotope effect if $m_l \neq 0$ are allowed by the reaction. But in the case of $He^+ + H^-$, it is a $1s$ electron that is transferred from H^-, meaning the $m_l = 0$ condition is satisfied.

One should also note that, if several molecular symmetries are involved, the following analysis might also be more complicated as there is a Landau-Zener window for each of them. In the $He^+ + H^-$ case, only the $^2\Sigma^+$ symmetry is involved, which further simplifies the treatment of the isotope effect.

Hence, for a given MN reaction between two ions whose reduced mass is μ and with N output channels k, there are N values of ζ_k. By evaluating $G(\zeta_k)$ as a function of the internuclear distance (see Appendix A), one can see that $E_{ic}^2/\Delta F$ monotonically decreases with the internuclear distance, meaning that for small internuclear distance $\zeta_k > 0.424$ while for greater internuclear distance $\zeta_k < 0.424$, i.e., there are states situated above and below the maximum of $G(\zeta)$.

Another consequence of this $G(\zeta)$ maximum, combined with the monotonic decrease of $E_{ic}^2/\Delta F$, is the presence of an optimum energy in the KER spectra. This optimum is called the Landau-Zener window. Previous experiments [35] have shown that this window ranges from 0.5 to 3 eV, but it varies as a function of the electron affinity of the anion, i.e., higher KER is favored when the electron affinity increases.

Unfortunately, another effect might counterbalance this general tendency: one can see in Fig. 3 that—at a given internuclear distance—the interaction potential also depends on the orbital momentum. Therefore, it is not possible to estimate, using only the KER and the electron affinity, the value of $E_{ic}^2/\Delta F$ for a given state. This dependency is strong enough to invalidate any prediction made using Olson's [51] fit over those values.

If one studies the same MN reaction with other isotopes whose reduced mass is μ', then for each channel

$$\zeta_k' = \sqrt{\mu'/\mu}\zeta_k. \tag{10}$$

This means that all channels are shifted by the same factor. Heavier isotopes have higher ζ_k values than lighter ones.

Some channels are above and others are below the maximum of $G(\zeta)$. Therefore, for heavier isotopes, the partial cross section of the channels above the maximum (lower excited states) decreases, while the partial cross section of the channels below the maximum (higher excited states) increases. As a result, there is no trivial dependency on μ for the total cross section. Nevertheless, this global increase of the ζ_k values for heavier isotopes systematically favors the higher excited states, i.e., heavier isotopes tend to favor lower kinetic-energy release products.

This effect is equivalently explained as follows: When two ions collide, they reach the crossing distance twice (approach and departure). In order to neutralize, they should cross ($\propto e^{-\zeta}$) and avoid the crossing ($\propto 1 - e^{-\zeta}$). The product of those two, integrated over all the impact parameters, leads to Eqs. (1) and (3). One can identify two extreme cases: for the first one, the interaction term is small (higher excited states), i.e., the system passes through the crossing most of the time; for the other one, the interaction term is large (lower excited states), i.e., the crossing is mostly avoided. As a consequence, as the kinetic energy at each crossing is fixed ($=E_{\mathrm{KER}}$), the heavier isotopes reach those crossings at a slower radial velocity, meaning that they spend more time through the crossing and increase the probability to avoid it. Therefore, the products with a low avoided crossing probability are favored by those heavier isotopes, i.e., the higher excited states are favored by heavier isotopes.

This argument applies directly to the $He^+ + H^-/D^-$ case (Fig. 4): The increase of μ leads to an increase of ζ for $He^+ + D^-$ (1.33 a.m.u.) compared to the one for $He^+ + H^-$ (0.8 a.m.u.), which favors the higher excited states of helium ($1s3s\ ^1S$, $1s3p\ ^3P^o$) compared to the lesser excited state ($1s3s\ ^3S$) situated above the $G(\zeta)$ maximum.

One should note that the branching ratios for the $3d\ ^{1,3}D$ states remain rather constant between the two reactions. This is explained by the nonlinearity of the $G(\zeta)$ function. The partial cross section increases less for those states that for the $3p\ ^3P^o$ one.

VI. CONCLUSION

By establishing that the two-channel Landau-Zener model applied to the anion-centered asymptotic model interaction terms is sufficient to reproduce the $He^+ + H^-/D^-$ mutual neutralization isotope effect, we were able to define a low collision energy regime for the MN reaction.

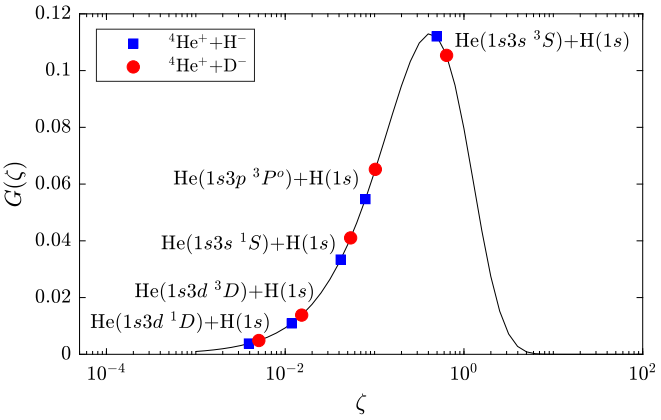

FIG. 4. Isotope effect on the branching ratios of the $He^+ + H^-$ MN reaction illustrated by the $G(\zeta)$ function. The values for E_{ic} are given by the anion-centered asymptotic model.

Within that regime, we have shown that the collision energy does not affect the branching ratios of the reaction. As most of the published experimental branching ratios were measured at a collision energy below 50 meV, the low collision energy condition is satisfied, which means that the branching ratio remains constant (and remains valid for reaction rates below 1000 K). The partial cross section is inversely proportional to the collision energy with a nonlinear effect of the isotope on its magnitude. Hence, the best way to show the cross sections for small collision energy is to show them as a function of the collision energy (without a factor μ which would complexify the analysis).

We have also used the Landau-Zener window scheme, which defines a KER range where the partial cross section for the neutral products is maximum, and deduced that heavier isotopes tend to favor higher excited states, i.e., lower kinetic-energy release states.

ACKNOWLEDGMENTS

This work was supported by Fonds De La Recherche Scientifique – FNRS Grant No. 4.4504.10. The authors thank the Belgian State for the grant allocated by Royal Decree for research in the domain of controlled thermonuclear fusion. A.D. is supported by the Swedish National Infrastructure, DESIREE (Swedish Research Council Contracts No. 2017-00621 and No. 2021-00155). X.U. is a Senior Research Associate of the Fonds de la Recherche Scientifique – FNRS. This paper is based upon work from COST Action CA18212—Molecular Dynamics in the GAS phase (MD-GAS), supported by COST (European Cooperation in Science and Technology). V.M.A. is supported by NSF Grant No. PHY-1530944.

APPENDIX A: ANION-CENTERED ASYMPTOTIC MODEL

The ACAM is a linear combination of atomic orbitals which considers only one active electron shell for the neutralized atom and one active shell for the anion (the wave functions are antisymmetrized). This model is asymptotic; it considers only the exponential part of the radial wave

function evaluated on a spherical surface around the anion core [44], meaning that it is valid only when the internuclear distance is larger than 10 Bohr radii. In such case the mean position of the atoms corresponds to the position of the nuclei.

The interaction term is evaluated at the crossing between flat covalent (He^0H^0) potential energy curves and the ionic (He^+H^-) curve given by Eq. (B4). Such approximations are valid for large internuclear distances.

The interaction potential predicted by this model is

$$
\begin{aligned}
E_{ic}(\Lambda,S) = (-1)^{N_{A+}+N_{B0}+S_{\rm mo}+S_{A+}+S_{B-}} \sqrt{N_{A0}N_{B-}}\, G^{SA0,LA0}_{SA+,LA+}\; G^{SB-,LB-}_{SB0,LB0} [(2S_{A0}+1)(2S_{B-}+1)]^{1/2} \begin{Bmatrix} S_{A+} & 1/2 & S_{A0} \\ S_{B0} & S_{\rm mo} & S_{B-} \end{Bmatrix} \\
\times \sum_{\tilde{\Lambda}} \sum_{\substack{m_{LA+},m_{LB0} \\ m_{LA0},m_{LB-} \\ m_l}} \begin{bmatrix} L_{A+} & l_{A0} & L_{A0} \\ m_{LA+} & m_l & m_{LA0} \end{bmatrix} \begin{bmatrix} L_{B0} & l_{B-} & L_{B-} \\ m_{LB0} & m_l & m_{LB-} \end{bmatrix} \left(\frac{1}{\sqrt{\text{no. } L_{\rm ion}}} \sum_{L_{\rm ion}} \begin{bmatrix} L_{A+} & L_{B-} & L_{\rm ion} \\ m_{LA+} & m_{LB-} & \tilde{\Lambda} \end{bmatrix} \right) \\
\times \left(\frac{1}{\sqrt{\text{no. } L_{\rm cov}}} \sum_{L_{\rm cov}} \begin{bmatrix} L_{A0} & L_{B0} & L_{\rm cov} \\ m_{LA0} & m_{LB0} & \tilde{\Lambda} \end{bmatrix} \right) \frac{\gamma_A (2\gamma_A)^{1/\gamma_A} R_x^{-1+1/\gamma_A} e^{-\gamma_A R_x}}{\sqrt{\Gamma\left(\gamma_A^{-1}+l_A+1\right)\Gamma\left(\gamma_A^{-1}-l_A\right)}} \\
\times A_{B^-} \frac{(m_l+1)}{(2\gamma_B R_x)^{|m_l|}\,|m_l|!} \sqrt{\frac{(2l_A+1)}{2}\frac{(l_A+|m_l|)!}{(l_A-|m_l|)!}} \sqrt{\frac{(2l_B+1)}{2}\frac{(l_B+|m_l|)!}{(l_B-|m_l|)!}}.
\end{aligned}
\tag{A1}
$$

Here, N is the number of valence electrons, L is the atomic orbital momentum and "no. L" is the number of values it may take, S is the atomic spin, l is the angular momentum of the valence electron, $S_{\rm mo}$ is the spin of the quasimolecule, $\Lambda = |\tilde{\Lambda}|$ is the projection of its orbital momentum, all m's correspond to the projection of their quantum numbers along the internuclear axis, and $m_l = m_{lA0} = m_{lB-}$. The A^+, A^0, B^0, and B^- indices indicate the atom which the quantum number refers to (A = He, B = H/D). $G^{S',L'}_{S,L}$ are the coefficients of fractional parentage, $\begin{bmatrix} j_1 & j_2 & j_3 \\ m_1 & m_2 & m_3 \end{bmatrix}$ are the Clebsh-Gordan coefficients, $\begin{Bmatrix} j_1 & j_2 & j_3 \\ j_4 & j_5 & j_6 \end{Bmatrix}$ are the Wigner $6-j$ symbols, $\gamma^2/2$ is the binding energy of the valence electron (when attached to the atom A or B), $\Gamma(z)$ is the gamma function, and $A_{B^-} = 0.791$ is the asymptotic normalization factor of the anion wave function for hydrogen (as suggested by Barklem [45]). The interaction potentials are given in Table II.

TABLE II. $He^+ + H^-$ branching ratios at 10-meV collision energy. The columns are named by the dynamics-solving method indicated and the anion isotope as an index. The interaction potential is given for the $^2\Sigma^+$ symmetry.

He	E_{ic}	ACAM branching ratios (%)			
state	(a.u.)	SLZ_H	MLZ_H	SLZ_D	MLZ_D
$2s\ ^3S$	1.449×10^{-2}	0.14	0.00	0.02	0.00
$2s\ ^1S$	6.586×10^{-3}	5.25	0.00	2.25	0.00
$2p\ ^3P^o$	1.145×10^{-2}	0.02	0.00	0.00	0.00
$2p\ ^1P^o$	5.859×10^{-3}	3.48	3.54	1.15	1.08
$3s\ ^3S$	8.231×10^{-4}	43.70	48.55	38.84	43.00
$3s\ ^1S$	1.881×10^{-4}	12.59	12.17	14.80	14.11
$3p\ ^3P^o$	2.291×10^{-4}	23.58	24.66	26.83	28.27
$3d\ ^3D$	8.001×10^{-5}	4.87	5.01	5.92	6.09
$3d\ ^1D$	4.605×10^{-5}	1.68	1.70	2.07	2.09
$3p\ ^1P^o$	7.160×10^{-5}	4.19	4.37	5.10	5.35
$4s\ ^3S$	2.728×10^{-11}	0.00	0.00	0.00	0.00

The details of the modification applied to this formula with respect to the formulation of Janev [44] are the subject of a forthcoming paper. But the modifications applied here do not change the value of the interaction term in the Σ symmetries with $m_l = 0$. Hence both formulas are interchangeable in the $He^+ + H^-$ case.

While it is difficult to give a general description of the interaction term as a function of the internuclear distance, it is possible to describe its tendency as a function R_x. Considering that the binding energy of the anion remains constant, recalling that

$$
E_{\rm KER} = \frac{\gamma_A^2}{2} - \frac{\gamma_B^2}{2} = \frac{1}{R_x}, \tag{A2}
$$

looking only at the component of Eq. (A1) which depends on R_x and γ_A, and finally applying the $\Delta F \simeq 1/R_x^2$ factor to it, one can obtain the tendency shown in Fig. 3.

This model is not suited to describe other processes happening at shorter internuclear distance (<10 Bohr radii), such as associative ionization (AI) and transfer ionization. But for $He^+ + H^-$ MN, the low impact parameters, which allow reaching short internuclear distances, have negligible contributions. Autoionization widths have been computed by Larson *et al.* [4] and found to be negligible beyond 4 Bohr radii. This is to be compared with the location of the important avoided crossings leading to $He(n=3) + H$, i.e., 25 Bohr radii. Another way to gauge the importance of autoionization is to compare AI (corresponding to $HeH^+ + e^-$ products) and MN cross sections. AI was found [52] to be three orders of magnitude less efficient than MN at similar collision energies.

The main limitation of the present model is the absence of treatment of the configuration mixing for the active electron, which might play a major role in MN reactions where transitions are configuration forbidden, such as $N^+ + O^-$ [39,53]. Such configuration mixing is not critical for $He^+ + H^-$ MN.

APPENDIX B: MULTICHANNEL LANDAU-ZENER FORMULA

In the multichannel Landau-Zener model for N covalent states, $P_k(b)$, the transition probability—as a function of the impact parameter b—between the ionic curve and the kth covalent state (counting from the most distant crossing), is given by [47]:

$$\begin{aligned} P_k &= p_1 p_2 \cdots p_{k-1} \times p_k(1-p_k) \times \left[1 + (1-p_{k+1})^2 + p_{k+1}^2(1-p_{k+2})^2 + p_{k+1}^2 (p_{k+2})^2 (1-p_{k+3})^2 \right. \\ &\quad \left. + p_{k+1}^2 \cdots p_{N-1}^2 (1-p_N)^2 + p_{k+1}^2 \cdots - p_N^2 \right] \quad \text{if } k < N-1 \\ &= p_1 p_2 \cdots p_{k-1} \times p_k(1-p_k) \times \left[1 + p_N^2 + (1-p_N)^2\right] \quad \text{if } k = N-1 \\ &= p_1 p_2 \cdots p_{k-1} \times p_k(1-p_k) \times [1+1] \ \text{ if } k = N \end{aligned} \tag{B1}$$

where

$$p_k = \exp\left(-\frac{-2\pi E_{ic,k}^2}{\hbar v_{R,k}(b) \Delta F_k}\right), \tag{B2}$$

and $v_{R,k}$ is the radial velocity.

Therefore, the partial cross section $\sigma_{\mathrm{MLZ},k}$ for the kth state is given by

$$\sigma_{\mathrm{MLZ},k} = 2\pi \int_0^{b_{\max,k}} P_k(b)\, b db \tag{B3}$$

where $b_{\max,k} = R_{c,k}\sqrt{1 - V_k(R_{c,k})/E_0}$ is the maximum impact parameter.

The potential for the ionic curve in the multichannel Landau-Zener model incorporates the polarizability of the ions:

$$V_{i,\mathrm{MLZ}}(R) = -\frac{1}{R} - \frac{\alpha_{\mathrm{H}^-} + \alpha_{\mathrm{He}^+}}{4R^4} \tag{B4}$$

where $\alpha_{\mathrm{H}^-} = 216$ and $\alpha_{\mathrm{He}^+} = 0.294$ are the static polarizabilities of $\mathrm{H}^-(\mathrm{D}^-)$ and He^+, respectively [54].

In order to keep the two-channel Landau-Zener model analytical, the ionic potential is kept purely Coulombic:

$$V_{i,\mathrm{SLZ}}(R) = -\frac{1}{R}. \tag{B5}$$

While those two models give slightly different branching ratios (Table II), the main difference concerns the He($2s$) states. This difference comes from a combination of the flux redistribution effect of the MLZ combined – to a smaller extent – with the $1/R^4$ component of the ionic potential. At any rate, as the overall tendency remains the same, we can describe the collision using the two-channel Landau-Zener model.

The impact parameter b approximation of the MLZ model was chosen—instead of the total angular momentum J general case—to be as close as possible to Eq. (1), incorporating all output channels at the same time instead of separately.

This approximation is valid when the amount of J involved in the collision is sufficiently high. One could argue that it is not the case at low collision energies, but the MN reaction is a special collision: It is exothermic and, before the collision, the two ions are attracted by the Coulomb $1/R$ potential. This potential dominates the centrifugal term $J(J+1)/2\mu R^2$ at large internuclear distance up to a value $J_{\max}$ such that

$$\frac{J_{\max}(J_{\max}+1)}{2\mu R_c^2} = \left(E_{r,i} + \frac{1}{R_c}\right). \tag{B6}$$

It means that when the collision energy decreases the amount of available J remains identical instead of decreasing. For $\mathrm{He}^+ + \mathrm{H}^-$ with an avoided crossing situated at 25 Bohr radii, i.e., $\mathrm{He}(n=3) + \mathrm{H}(1s)$, one finds $J_{\max} \geqslant \sqrt{2\mu R_c} = 271$, which justifies the approximation $J = \sqrt{2\mu E_{r,i}} b$ and the replacement of the sum over J by an integral.

While the value of $J_{\max}$ scales with the square root of the reduced mass, this scaling has no influence on the cross section. Indeed, assuming the S-matrix elements slowly depend on J, the quantum expression of the cross section reads

$$\sigma = \frac{\pi}{2\mu E_{r,i}} \sum_{J=0}^{J_{\max}} (2J+1)|S_{ic}|^2 \simeq \frac{\pi}{2\mu E_{r,i}} \left|\bar{S}\right|^2 (J_{\max}+1)^2. \tag{B7}$$

Combining Eqs. (B6) and (B7), we may rewrite the cross section as

$$\sigma \simeq \pi \left|\bar{S}\right|^2 R_c^2 \left(1 + \frac{1}{E_{r,i} R_c}\right)$$

which does not depend on the reduced mass except through the reaction probability (squared matrix S element).

[1] P. S. Barklem, Accurate abundance analysis of late-type stars: Advances in atomic physics, Astron. Astrophys. Rev. **24**, 9 (2016).

[2] K. Lind, T. Nordlander, A. Wehrhahn, M. Montelius, Y. Osorio, P. S. Barklem, M. Afsar, C. Sneden, and C. Kobayashi, Non-LTE abundance corrections for late-type stars from 2000 Å to 3 μm. I. Na, Mg, and Al, Astron. Astrophys. **665**, A33 (2022).

[3] J. Hörnquist, P. Hedvall, A. Larson, and A. E. Orel, Mutual neutralization in $\mathrm{H}^+ + \mathrm{H}^-$ collisions: An improved theoretical model, Phys. Rev. A **106**, 062821 (2022).

[4] A. Larson, S. M. Nkambule, and A. E. Orel, Theoretical study of mutual neutralization in $\mathrm{He}^+ + \mathrm{H}^-$ collisions, Phys. Rev. A **94**, 022709 (2016).

[5] S. M. Nkambule, N. Elander, A. Larson, J. Lecointre, and X. Urbain, Differential and total cross sections of mutual

neutralization in low-energy collisions of isotopes of $H^+ + H^-$, Phys. Rev. A **93**, 032701 (2016).

[6] T. Launoy, J. Loreau, A. Dochain, J. Liévin, N. Vaeck, and X. Urbain, Mutual neutralization in Li^+-D^- collisions: A combined experimental and theoretical study, Astrophys. J. **883**, 85 (2019).

[7] H. M. Hedberg, S. Nkambule, and Å. Larson, Landau–zener studies of mutual neutralization in collisions of $H^+ + H^-$ and $Be^+ + H^-$, J. Phys. B **47**, 225206 (2014).

[8] M. Guitou, A. Spielfiedel, D. Rodionov, S. Yakovleva, A. Belyaev, T. Merle, F. Thévenin, and N. Feautrier, Quantum chemistry and nuclear dynamics as diagnostic tools for stellar atmosphere modeling, Chem. Phys. **462**, 94 (2015).

[9] A. K. Belyaev and Y. V. Voronov, Inelastic processes in low-energy sulfur-hydrogen collisions, Astrophys. J. **893**, 59 (2020).

[10] S. A. Yakovleva, A. K. Belyaev, and M. Bergemann, Cobalt-hydrogen atomic and ionic collisional data, Atoms **8**, 34 (2020).

[11] A. K. Belyaev, D. V. Vlasov, A. Mitrushchenkov, and N. Feautrier, Quantum study of inelastic processes in low-energy calcium-hydrogen collisions, Mon. Notices Royal Astron. Soc **490**, 3384 (2019).

[12] A. K. Belyaev, Y. V. Voronov, A. Mitrushchenkov, M. Guitou, and N. Feautrier, Inelastic processes in oxygen-hydrogen collisions, Mon. Notices Royal Astron. Soc **487**, 5097 (2019).

[13] A. Mitrushchenkov, M. Guitou, A. K. Belyaev, Y. V. Voronov, and N. Feautrier, Inelastic excitation and charge transfer processes for oxygen in collision with H atoms, J. Chem. Phys. **150**, 064312 (2019).

[14] S. Yakovleva, A. Belyaev, and W. Kraemer, Inelastic processes in low-energy iron-hydrogen collisions, Chem. Phys. **515**, 369 (2018).

[15] A. K. Belyaev and S. A. Yakovleva, Data on inelastic processes in low-energy collisions of barium atoms and ions with hydrogen atoms and anions, Mon. Notices Royal Astron. Soc **478**, 3952 (2018).

[16] S. A. Yakovleva, P. S. Barklem, and A. K. Belyaev, Data on inelastic processes in low-energy potassium-hydrogen and rubidium-hydrogen collisions, Mon. Notices Royal Astron. Soc **473**, 3810 (2018).

[17] A. K. Belyaev and Y. V. Voronov, Atomic data on inelastic processes in low-energy manganese-hydrogen collisions, Astron. Astrophys. **606**, A106 (2017).

[18] A. Mitrushchenkov, M. Guitou, A. K. Belyaev, S. A. Yakovleva, A. Spielfiedel, and N. Feautrier, Calcium-hydrogen interactions for collisional excitation and charge transfer, J. Chem. Phys. **146**, 014304 (2017).

[19] S. A. Yakovleva, Y. V. Voronov, and A. K. Belyaev, Atomic data on inelastic processes in low-energy beryllium-hydrogen collisions, Astron. Astrophys. **593**, A27 (2016).

[20] A. K. Belyaev, S. A. Yakovleva, M. Guitou, A. O. Mitrushchenkov, A. Spielfiedel, and N. Feautrier, Model estimates of inelastic calcium-hydrogen collision data for non-LTE stellar atmospheres modeling, Astron. Astrophys. **587**, A114 (2016).

[21] A. K. Belyaev, B. Lepetit, and F. X. Gadéa, Theoretical study of electronic excitation, ion-pair formation, and mutual neutralization in cesium-hydrogen collisions, Phys. Rev. A **90**, 062701 (2014).

[22] A. K. Belyaev, S. A. Yakovleva, and P. S. Barklem, Inelastic silicon-hydrogen collision data for non-LTE applications in stellar atmospheres, Astron. Astrophys. **572**, A103 (2014).

[23] A. K. Belyaev, Inelastic aluminium-hydrogen collision data for non-LTE applications in stellar atmospheres, Astron. Astrophys. **560**, A60 (2013).

[24] A. K. Belyaev, Model approach for low-energy inelastic atomic collisions and application to Al + H and $Al^+ + H^-$, Phys. Rev. A **88**, 052704 (2013).

[25] P. S. Barklem, A. K. Belyaev, A. Spielfiedel, M. Guitou, and N. Feautrier, Inelastic Mg + H collision data for non-LTE applications in stellar atmospheres, Astron. Astrophys. **541**, A80 (2012).

[26] A. K. Belyaev, P. S. Barklem, A. Spielfiedel, M. Guitou, N. Feautrier, D. S. Rodionov, and D. V. Vlasov, Cross sections for low-energy inelastic Mg + H and $Mg^+ + H^-$ collisions, Phys. Rev. A **85**, 032704 (2012).

[27] P. S. Barklem, A. K. Belyaev, A. S. Dickinson, and F. X. Gadéa, Inelastic Na + H collision data for non-LTE applications in stellar atmospheres, Astron. Astrophys. **519**, A20 (2010).

[28] A. K. Belyaev, P. S. Barklem, A. S. Dickinson, and F. X. Gadéa, Cross sections for low-energy inelastic H + Na collisions, Phys. Rev. A **81**, 032706 (2010).

[29] J. Grumer and P. S. Barklem, Excitation and charge transfer in low-energy hydrogen atom collisions with neutral manganese and titanium, Astron. Astrophys. **637**, A28 (2020).

[30] P. S. Barklem, A. M. Amarsi, J. Grumer, G. Eklund, S. Rosén, M. Ji, H. Cederquist, H. Zettergren, and H. T. Schmidt, Mutual neutralization in $Li^+ + H^-/D^-$ and $Na^+ + H^-/D^-$ collisions: Implications of experimental results for non-LTE modeling of stellar spectra, Astrophys. J. **908**, 245 (2021).

[31] A. M. Amarsi and P. S. Barklem, Excitation and charge transfer in low-energy hydrogen atom collisions with neutral carbon and nitrogen, Astron. Astrophys. **625**, A78 (2019).

[32] P. S. Barklem, Excitation and charge transfer in low-energy hydrogen atom collisions with neutral oxygen, Astron. Astrophys. **610**, A57 (2018).

[33] P. S. Barklem, Excitation and charge transfer in low-energy hydrogen atom collisions with neutral iron, Astron. Astrophys. **612**, A90 (2018).

[34] X. Urbain, J. Lecointre, F. Mezdari, K. A. Miller, and D. W. Savin, Merged-beam study of mutual neutralization of H^- and H^+, J. Phys.: Conf. Ser. **388**, 092004 (2012).

[35] X. Urbain, N. de Ruette, A. Dochain, T. Launoy, R. F. Nascimento, M. Kaminska, M. H. Stockett, J. Loreau, J. Liévin, N. Vaeck, R. Thomas, H. Schmidt, and H. Cederquist, Merged beam studies of mutual neutralization at subthermal collision energies, J. Phys.: Conf. Ser. **1412**, 062009 (2020).

[36] G. Eklund, J. Grumer, S. Rosén, M. C. Ji, N. Punnakayathil, A. Källberg, A. Simonsson, R. D. Thomas, M. H. Stockett, P. Reinhed, P. Löfgren, M. Björkhage, M. Blom, P. S. Barklem, H. Cederquist, H. Zettergren, and H. T. Schmidt, Cryogenic merged-ion-beam experiments in DESIREE: Final-state-resolved mutual neutralization of Li^+ and D^-, Phys. Rev. A **102**, 012823 (2020).

[37] G. Eklund, J. Grumer, P. S. Barklem, S. Rosén, M. C. Ji, A. Simonsson, R. D. Thomas, H. Cederquist, H. Zettergren, and H. T. Schmidt, Final-state-resolved mutual neutralization of na^+ and d^-, Phys. Rev. A **103**, 032814 (2021).

[38] J. Grumer, G. Eklund, A. M. Amarsi, P. S. Barklem, S. Rosén, M. C. Ji, A. Simonsson, H. Cederquist, H. Zettergren, and H. T. Schmidt, State-resolved mutual neutralization of Mg^+ and D^-, Phys. Rev. Lett. **128**, 033401 (2022).

[39] N. de Ruette, A. Dochain, T. Launoy, R. F. Nascimento, M. Kaminska, M. H. Stockett, N. Vaeck, H. T. Schmidt, H. Cederquist, and X. Urbain, Mutual neutralization of O^- with O^+ and N^+ at subthermal collision energies, Phys. Rev. Lett. **121**, 083401 (2018).

[40] R. D. Thomas, H. T. Schmidt, G. Andler, M. Björkhage, M. Blom, L. Brännholm, E. Bäckström, H. Danared, S. Das, N. Haag, P. Halldén, F. Hellberg, A. I. S. Holm, H. A. B. Johansson, A. Källberg, G. Källersjö, M. Larsson, S. Leontein, L. Liljeby, P. Löfgren *et al.*, The double electrostatic ion ring experiment: A unique cryogenic electrostatic storage ring for merged ion-beams studies, Rev. Sci. Instrum. **82**, 065112 (2011).

[41] A. F. Schmidt-May, S. Rosén, M. Ji, G. Eklund, H. Zettergren, H. Cederquist, H. T. Schmidt, P. S. Barklem, and J. Grumer, companion paper, Observation of an isotope effect in state-selective mutual neutralization of lithium with hydrogen, Phys. Rev. A **108**, 042810 (2023).

[42] A. Kramida, Yu. Ralchenko, J. Reader, and and NIST ASD Team, NIST Atomic Spectra Database, version 5.10, https://physics.nist.gov/asd [2023 March 1], National Institute of Standards and Technology, Gaithersburg, MD (2022)

[43] See Supplemental Material at http://link.aps.org/supplemental/10.1103/PhysRevA.108.042809 for the partial cross sections and the reaction rates computed with the $ACAM_{MLZ}$ model.

[44] R. Janev, *Nonadiabatic Transitions Between Ionic and Covalent States* (Academic, New York, 1976), pp. 1–37.

[45] P. S. Barklem, Correspondence between the surface integral and linear combination of atomic orbitals methods for ionic-covalent interactions in mutual neutralization processes involving H^-/D^-, Phys. Rev. A **104**, 062806 (2021).

[46] C. Zener, Non-adiabatic crossing of energy levels, Proc. R. Soc. A **137**, 696 (1932).

[47] A. Salop and R. E. Olson, Charge exchange between H(1*s*) and fully stripped heavy ions at low-keV impact energies, Phys. Rev. A **13**, 1312 (1976).

[48] L. D. Landau, Zur Theorie der Energieubertragung. II, Phys. Z. Sowjetunion **2**, 46 (1932).

[49] E. C. G. Stückelberg, Theorie der unelastischen Stösse zwischen Atomen, Helv. Phys. Acta **5**, 369 (1932).

[50] A. K. Belyaev and Y. V. Voronov, Isotopic effects in low-energy lithium-hydrogen collisions, Phys. Rev. A **104**, 022812 (2021).

[51] R. E. Olson, Absorbing-sphere model for calculating ion-ion recombination total cross sections, J. Chem. Phys. **56**, 2979 (1972).

[52] A. L. Padellec, T. Launoy, A. Dochain, and X. Urbain, Investigation of critical parameters controlling the efficiency of associative ionization, J. Phys. B **50**, 095202 (2017).

[53] M. Poline, S. Rosén, M. C. Ji, A. Simonsson, P. Reinhed, M. Larsson, H. T. Schmidt, R. D. Thomas, A. Dochain, X. Urbain, J. Grumer, P. S. Barklem, S. G. Ard, N. S. Shuman, and A. A. Viggiano, Storage-ring study of the mutual neutralization of N^+ with O^-, Phys. Rev. A **105**, 062825 (2022).

[54] T. Gould and T. Bučko, C6 coefficients and dipole polarizabilities for all atoms and many ions in rows 1–6 of the periodic table, J. Chem. Theory Comput. **12**, 3603 (2016).